IEEE Access
Multidisciplinary | Rapid Review | Open Access Journal

SPECIAL SECTION ON ADVANCED CONTROL AND HEALTH MANAGEMENT FOR AIRCRAFT AND ITS PROPULSION SYSTEM

Received September 2, 2018, accepted September 24, 2018, date of publication October 1, 2018, date of current version October 25, 2018.

Digital Object Identifier 10.1109/ACCESS.2018.2873292

A Robust SINS/VO Integrated Navigation Algorithm Based on RHCKF for Unmanned Ground Vehicles

YA ZHANG, FEI YU, YANYAN WANG, AND KAI WANG
School of Electrical Engineering and Automation, Harbin Institute of Technology, Harbin 150001, China

Corresponding author: Fei Yu (yufei@hit.edu.cn)

This work was supported in part by the National Natural Science Foundation of China under Grant 51709068, Grant 51809056, and Grant 51679047, and in part by the Postdoctoral Foundation of Heilongjiang Province under Grant LBH-Z16044.

ABSTRACT High precision localization information is the precondition of unmanned ground vehicles. But the global navigation satellite system (GNSS) signal turns unreliable in urban and forest areas since it is blocked by buildings and trees easily, which causes decline of localization accuracy. In order to solve this problem, an integrated navigation system based on the strapdown inertial navigation system and binocular camera visual odometer is utilized in this paper to provide navigation parameters for unmanned ground vehicles when the GNSS signal denies. However, the existing integrated navigation algorithm cannot meet the requirement of the high precision localization for unmanned ground vehicles because of the uncertainty and nonlinearity. As a result, a robust nonlinear filter based on the H_∞ filter and the cubature Kalman filter, named RHCKF, is proposed in this paper, adopted in unmanned vehicle navigation. Simulation and real test are both carried out to verify the effectiveness of the novel navigation algorithm when the GNSS signal denies.

INDEX TERMS Unmanned ground vehicle, strapdown inertial navigation system, visual odometer, integrated navigation, robust filter, nonlinear filter.

I. INTRODUCTION

With the rapid development of the autonomous navigation and control technologies, the unmanned ground vehicles has been widely used both in military and civilian such as transportation, rescue, investigation, explosive disposal and so on [1]–[4]. No matter what kinds of purpose, accurate navigation information is the precondition. As a result, the navigation technique of unmanned ground vehicles is becoming the significant research orientation of unmanned vehicles.

Nowadays, various navigation systems, including Global Navigation Satellite System (GNSS), Strapdown Inertial Navigation System (SINS) and Visual Odometer (VO), have been equipped in unmanned vehicles [5], [6]. But they have limitations in different applications. The SINS is the most widely used in modern navigation thanks to its autonomous, compact and low-cost. However, its navigation accuracy will decrease inevitably due to the accumulative error of inertial components, especially in long-term navigation [2]. Despite the fact that the GNSS can correct the accumulative error of SINS by using its high signal-point positioning, it is easy be interfered by the surroundings or human factors, such as clouds, buildings or active jamming. So the GNSS has low precision or even cannot be used in urban areas [7]. The VO is the process of estimating the ego-motion of unmanned vehicles using image sequences captured by the camera equipped on it [8]. Thus, the accuracy of the VO algorithm relies on the quality of image sequences which is influenced by the surrounding. As a result, any single of these navigation systems cannot meet the needs of unmanned ground vehicles.

Therefore, the integrated navigation system has attracted more and more attentions. In integrated navigation systems, the redundant and complementary measurements from different sensors can effectively improve the accuracy of the whole system. Taken the advantages of SINS and VO into account, we focus on the SINS/VO integrated navigation system when GNSS is denied to enhance its navigation performance and reliability in this paper.

It is well known that the essence of integrated navigation system is the optimal estimation, so the estimation algorithm is the conclusive and key factor in the SINS/VO integrated navigtion system. The most commonly used state estimation method is the Kalman filter (KF), which is a high efficiency

recursive filter. However, KF can only be used to deal with the linear system because of that the signal process is regarded as the output of the linear system. Due to large misalignment angles or other jolts in actual systems, nonlinearity does exist in SINS/VO integrated navigation systems. If linear KF is still used, the estimated error will be produced or even the filter divergent in practice [9]–[11]. Thus the nonlinear filter becomes the focus of research.

At present, there are plenty of nonlinear filters, such as Extend Kalman Filter (EKF), Unscented Kalman Filter (UKF) and Cubature Kalman filter (CKF) [12]–[17]. In EKF, the Taylor expansion is used to solve nonlinear state, but the filter precision is limited and calculating Jacobian matrix is complicated. Instead of practical linearization, the UKF uses the Unscented Transform (UT) to approximate the system distribution. But the UKF can not be used in high dimensional systems since its non-positive covariance matrix [13], [14]. So the CKF based on Cubature Transform (CT) was proposed to avoid the dimensionality curse. CKF is proposed to solve this nonlinear filtering problem on the basis of the spherical-radial cubature criterion. CKF approximates the mean and variance of probability distribution through a set of $2N$ (N is the dimension of the nonlinear system) Cubature points with the same weight firstly, then propagates the above cubature points through the nonlinear functions, and calculates the mean and variance of the current approximate Gaussian distribution by the propagated cubature points at last [14], [18], [19]. Due to its high precision and low calculation, the CKF is widely used to solve the nonlinearity problem in practical systems.

However, same as the KF, the CKF is based on the Bayesian estimation. That means, the estimation is optimal only when the statistical property are exactly known, which is difficult in practice. Besides, the noise model is time-varying actually because of the inertial sensors' error or low quality figures caused by illumination and many other reasons. As a result, the actual system has severe uncertainty. If traditional filters still be used, the reliability and accuracy cannot meet the requirement of unmanned vehicle navigation systems.

Aimed against the uncertainty problem, the robust filter algorithm has been considered to enhance the robustness of the SINS/VO integrated navigation system [12], [20]–[22]. Literature [23] investigated the tracking control problems for a class of uncertain nonlinear systems in lower triangular form, and to solve the uncertainty problem the adaptive neural control approach for nonlinear systems in presence of unmodeled dynamics nonlinear systems was presented in [24]–[26]. The H_∞ filter is a kind of robust filter method and it has good performance in restraining the modeling uncertainty and disturbance [21], [22], [27]. The Riccati Iteration algorithm based on robust H_∞ filter was proposed in [20]. And it has been successfully used in the SINS/Radar integrated navigation system whose statistical property of observation model is uncertain; [21] focused on the multiple satellites integrated navigation system with nonlinear system model and the robust filter method is used to estimate system states; [12], [28], [29] focused on a navigation system whose statistical property is unknown and a closed-loop robust H_∞ filter method has been used to enhance both the robustness and the filter accuracy. However, the initial parameters in the regular robust filter cannot reach the balance between the robustness and estimation accuracy which leads the filter algorithm has a large conservative property.

To solve the uncertainty and nonlinearity problems of actual systems, taken the advantages of the nonlinear CKF and robulst H_∞ filter into account, a novel SINS/VO integrated navigation algorithm based on nonlinear CKF and an adaptive H_∞ robust filter was proposed to enhance the system accuracy and adaptivity. In this manuscript, the nonlinear system model of SINS/VO integrated systems was built up to enhance the positioning accuracy of the integrated navigation system, and then we give the novel algorithm framework. In this novel algorithm, the CKF is used to deal with the system nonlinearity while the adaptive H_∞ filter is used to solve the system uncertainty.

The main contributions of this paper are summarized as below.

1) To improve the positioning accuracy of the unmanned ground vehicle, an integrated navigation system based on the SINS and OV is proposed in this manuscript. Taken the nonlinearity into account, the nonlinear system equation of the SINS/VO integrated navigation system is derived.
2) An robust integrated navigation system algorithm based on the H_∞ filter and the CKF, named RHCKF algorithm, is proposed in this paper. This RHCKF algorithm not only has the capacity of processing nonlinearity but also is able to achieve great accuracy and robustness of the SINS/VO integrated navigation system for unmanned ground vehicles.

The rest of this manuscript is organized as follows. Section II presented the nonlinear model of the SINS/VO integrated navigation system while the improved RHCKF algorithm based on the robust H_∞ filter and nonlinear CKF method for SINS/VO integrated navigation systems is proposed in Section III. The simulation and experiment are shown in Section IV. Section V concludes this manuscript.

II. SYSTEM MODEL OF SINS/VO INTEGRATED NAVIGATION SYSTEM

A. ERROR MODEL OF STRAPDOWN INERTIAL NAVIGATION SYSTEM

Considering numerous advantages of SINS in the unmanned ground vehicle navigation, the SINS is usually used as the main system. To improve the system precision remarkably, the nonlinear error model of the SINS is derived here detailedly.

Traditional linear differential equations are used under the assumption that misalignment angles are small for simplicity and convenience. However, the system is nonlinear when misalignment angles are large caused by the vehicle's maneuvering or external disturbances. And estimated errors

will exist if the linear model is still used. Thus the general expression of the nonlinear attitude error equation of SINS is shown as follows:

$$\dot{\phi} = C_{\omega}^{-1}\left[\left(I - C_{n}^{n'}\right)\hat{\omega}_{in}^{n} + C_{n}^{n'}\delta\omega_{in}^{n} - C_{b}^{n'}\varepsilon^{b}\right] + C_{\omega}^{-1}C_{b}^{n'}W_{g}^{b} \tag{1}$$

wherein $\phi = [\phi_x\ \phi_y\ \phi_z]^{\top}$ is the Euler error angle vector, the direction cosine matrix from the navigation coordinate system (n) to the calculated navigation coordinate system (n') is $C_{n}^{n'}$. $C_{b}^{n'}$ denotes the direction cosine matrix from the vehicle coordinate system (b) to n', ε^{b} and W_{g}^{b} are the gyro constant drift vector and the corresponding zero-mean Gaussian white noise vector, respectively, $\hat{\omega}_{in}^{n}$ is the practical gyro measurement vector, ω_{in}^{n} is the rotating angular rate vector of n relative to the inertial coordinate system (i), $\delta\omega_{in}^{n}$ is the calculated error vector of ω_{in}^{n}. C_{ω} is an intermediate matrix. The gyro measurement vector is equal to $\hat{\omega}_{in}^{n} = \omega_{in}^{n} + \delta\omega_{in}^{n}$.

The direction cosine matrix $C_{n}^{n'}$ related to three rotations, so it can be written:

$$\begin{aligned} C_{n}^{n'} &= C_{\phi_y}C_{\phi_x}C_{\phi_z} \\ &= \begin{bmatrix} \cos\phi_y & 0 & -\sin\phi_y \\ 0 & 1 & 0 \\ \sin\phi_y & 0 & \cos\phi_y \end{bmatrix} \cdot \\ &\quad \begin{bmatrix} 1 & 0 & 0 \\ 0 & \cos\phi_x & \sin\phi_x \\ 0 & -\sin\phi_x & \cos\phi_x \end{bmatrix} \cdot \\ &\quad \begin{bmatrix} \cos\phi_z & \sin\phi_z & 0 \\ -\sin\phi_z & \cos\phi_z & 0 \\ 0 & 0 & 1 \end{bmatrix} \end{aligned} \tag{2}$$

In Eq. 1, the C_{ω} is an intermediate variable, and we have this:

$$C_{\omega}^{-1} = \frac{1}{\cos\phi_x} \cdot \begin{bmatrix} \cos\phi_y\cos\phi_x & 0 & \sin\phi_y\cos\phi_x \\ \sin\phi_y\sin\phi_x & \cos\phi_x & -\cos\phi_y\sin\phi_x \\ -\sin\phi_y & 0 & \cos\phi_y \end{bmatrix} \tag{3}$$

Suppose that the accelerometer error is composed of the constant bias error ∇^{b} and the zero-mean Gaussian white noise vector W_{a}^{b}. Ignored the gravity acceleration error, the SINS velocity error equation is given by:

$$\begin{aligned} \delta\dot{v}^{n} &= C_{b}^{n'}\hat{f}^{b} - C_{b}^{n}\hat{f}^{b} + C_{b}^{n}\nabla^{b} \\ &\quad - (2\delta\omega_{ie}^{n} + \delta\omega_{en}^{n})(\hat{v}^{n} - \delta v^{n}) \\ &\quad - (2\hat{\omega}_{ie}^{n} + \hat{\omega}_{en}^{n})\delta v^{n} + C_{b}^{n}W_{a}^{b} \end{aligned} \tag{4}$$

wherein $\hat{f}^{b}$ and δf^{b} denote the specific force vector and its corresponding error vector respectively, $\hat{\omega}_{ie}^{n}$ is the calculated Earth's rotating angular rate, $\hat{\omega}_{en}^{n}$ is the calculated angular rate vector, $\delta\omega_{ie}^{n}$ and $\delta\omega_{en}^{n}$ indicate the error vectors of $\hat{\omega}_{ie}^{n}$ and $\hat{\omega}_{en}^{n}$ respectively, $\hat{v}^{n}$ and δv^{n} denote velocity measurement vector and its corresponding error vector, and $C_{b}^{n} = C_{n'}^{n}C_{b}^{n'}$.

It is assumed that the inertial sensor error meets the combination of a constant bias and a random noise which satisfies zero-mean and Gaussian distribution. As a result, their differential equations are:

$$\begin{cases} \dot{\varepsilon}^{b} = 0 \\ \dot{\nabla}^{b} = 0 \end{cases} \tag{5}$$

Position error equations comprise the longitude error $\delta\lambda$ and the latitude error δL :

$$\begin{cases} \delta\dot{L} = \delta v_y / R_M \\ \delta\dot{\lambda} = \sec L\delta v_x / R_N + \sec L\tan L\delta L v_x / R_N \end{cases} \tag{6}$$

wherein R_M and R_N are the Earth's radii of the meridian circle and the prime vertical circle, respectively; λ and L are the longitude and latitude of a point of interest; v_x and v_y are the east and north velocities with their velocity errors δv_x and δv_y, respectively.

B. SYSTEM MODEL OF BINOCULAR CAMERA BASED VISUAL ODOMETER

Two independent cameras capture the environment scene simultaneously in the binocular camera VO system and then the environment features are extracted from two different figures by utilizing the feature extraction algorithm simultaneously. The features from different figures are matched by using the feature matching method and the depth information are obtained by the triangulation theory. As a result, the three dimensional coordinate of the features in the field-of-view can be calculated accurately and the visual images can be projected to the three-dimensional world finally.

The schematic of binocular camera VO system is shown as Fig.1. The feature M is denoted as (X, Y, Z) in the world frame and (x_c, y_c, z_c) in the camera frame. $o_1u_1v_1$ and $o_2u_2v_2$ denote the pixel coordinates of the left camera and the right camera, respectively. $o_lx_ly_l$ and $o_rx_ry_r$ denote the coordinates of the left image plane and the right image plane, respectively. The subscripts l and r denote left and right, respectively.

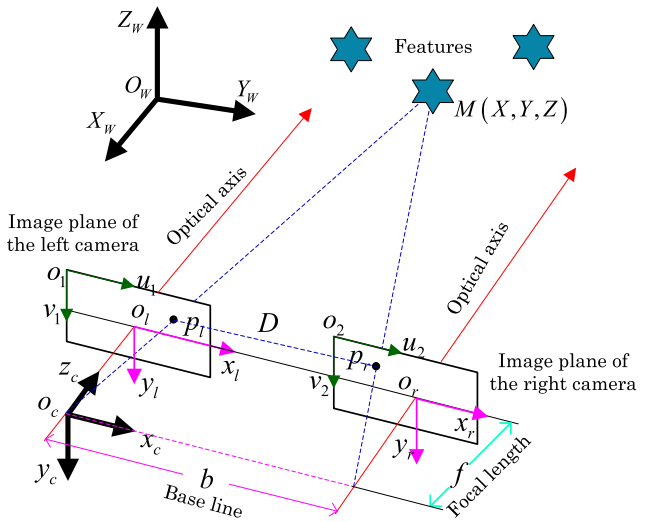

FIGURE 1. The schematic of binocular stereo imaging.

The coordinates o_l and o_r are represented as (u_{10}, v_{10}) and (u_{20}, v_{20}) in coordinates $o_1u_1v_1$ and $o_2u_2v_2$. The projected coordinates on the left and right image plane of feature are represented as $p_l(x_l, y_l)$ and $p_r(x_r, y_r)$, respectively. The baseline length which defined as the distance between two cameras' projection center is b. The optical axes of two cameras are parallel and vertical to the baseline. The focal length is f. $y_l = y_r$ when the two cameras are in the same plane. The image disparity of the two cameras is

$$D = x_l - x_r \tag{7}$$

The image disparity is a significant parameter which is used to transfer the feature point from the 2-D plane coordinate system to the 3-D camera coordinate system. It is known from the geometrical relationship that

$$\begin{cases} x_l = f\dfrac{x_c}{z_c} \\ x_r = f\dfrac{x_c - b}{z_c} \\ y_r = y_l = f\dfrac{y_c}{z_c} \end{cases} \tag{8}$$

As a result, the 3-D feature (x_c, y_c, z_c) in the camera coordinate can be obtained from

$$\begin{cases} x_c = \dfrac{x_l \cdot b}{D} \\ y_c = \dfrac{y \cdot b}{D} \\ z_c = \dfrac{f \cdot b}{D} \end{cases} \tag{9}$$

The relationship between the camera coordinate and the world coordinate is expressed as

$$\begin{bmatrix} X_W \\ Y_W \\ Z_W \end{bmatrix} = R \cdot \begin{bmatrix} x_c \\ y_c \\ z_c \end{bmatrix} + T \tag{10}$$

where R is a 3×3 orthogonal matrix which denotes the rotation matrix from the camera coordinate to the world coordinate; $T = [\,t_1\ t_2\ t_3\,]^\top$ denotes the translation matrix. In consideration of the transformation of coordinates and connecting adjacent motions, we can get the vehicle's velocity and pose relative to its original velocity, position and attitude.

From the above statement, it is obviously known that the feature extraction is one of the the most basic and vital techniques in VO systems. Nowadays, there are various feature extraction methods, such as the Harris feature extractor, the Binary Robust Independent Elementary Features (BRIEF), the Scale Invariant Feature Transform (SIFT), the Speeded Up Robust Features (SURF), the Features from Accelerated Segment Test (FAST) and the Oriented Rotated BRIEF (ORB) [5], [7]. Taken the real-time into consideration in actual applications, a feature extraction algorithm with low computation complexity should be taken into account. In FAST method, the gray values of a part of the pixel are compared to extract features instead of computing their gradients. Therefore, the computation complexity can be effectively reduced, improved the effectiveness of FAST feature extraction. Since the FAST method have been described in detail in [5], we will not be repeated. Hence, the FAST method introduced in [5] is used to extract features in this manuscript, assisted the SINS for navigation.

C. NONLINEAR FILTER EQUATION OF SINS/VO INTEGRATED NAVIGATION SYSTEM FOR UNMANNED GROUND VEHICLES

In this paper, the SINS and VO system are integrated to get more accurate navigation information for unmanned ground vehicles. In this SINS/VO integrated navigation system, the SINS is used as the main system to obtain the vehicle's motion while the VO is the aided system, which can get vehicle's velocity and pose to restrain filter errors, enhanced the accuracy of the integrated navigation system. The diagram of SINS/VO integrated navigation systems is shown as Fig. 2

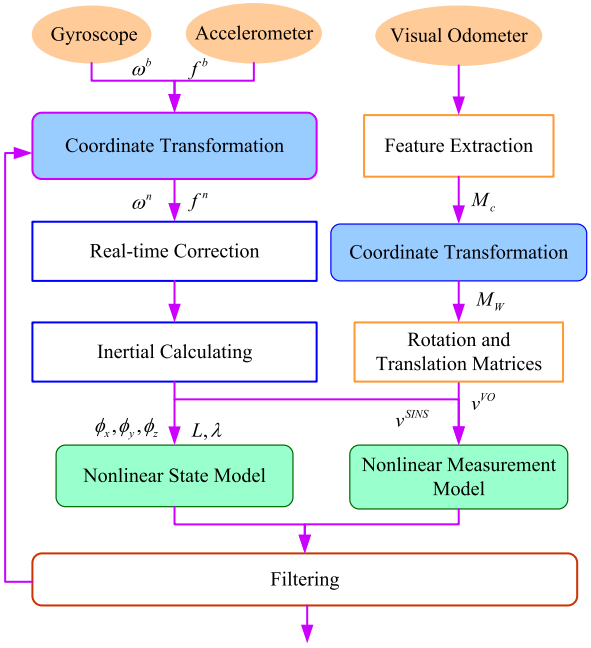

FIGURE 2. Diagram of the SINS/VO integrated navigation system.

The filter equations are established based on error models of SINS and VO system. Since we focus on unmanned ground vehicles, the altitude, the vertical velocity and the vertical acceleration are ignored. Thus, considered the position error, the velocity error, the attitude error and the inertial sensors' error, the state vector is denoted by Eq. 11 as follows:

$$X = [\delta\lambda\ \ \delta\varphi\ \ \delta v_x\ \ \delta v_y\ \ \phi_x\ \ \phi_y\ \ \phi_z\ \ \nabla_x\ \ \nabla_y\ \ \varepsilon_x\ \ \varepsilon_y\ \ \varepsilon_z]^\top \tag{11}$$

wherein, $\delta\lambda$ and $\delta\varphi$ are the longitude error and the latitude error, respectively; δv_x and δv_y represent the east and north velocity errors; ε_x and ε_y indicate the accelerometer bias in the horizontal direction; ε_x, ε_y and ε_z are the constant gyroscope drift; ϕ_x, ϕ_y and ϕ_z denote the attitude error.

On the basis of Eq. 1 $\sim$ Eq. 6, the differential equation of the position, velocity and attitude can be derived, expressed

as follows:

$$\begin{cases}
\delta\dot{L} = \dfrac{\delta v_y}{R_M} \\
\delta\dot{\lambda} = \dfrac{\delta v_x}{R_N}\sec L + \dfrac{\delta v_x}{R_N}\sec L\tan L \cdot L \\
\delta\dot{v}_x = -f_x(\cos\phi_z - 1) + f_y\sin\phi_z \\
\quad -f_z(\phi_y\cos\phi_z + \phi_x\sin\phi_z) \\
\quad + \dfrac{v_y}{R_M}\tan L\delta v_x + (2\omega_{ie}\sin L \\
\quad + \dfrac{v_x}{R_N}\tan L)\delta v_y + (2\omega_{ie}\cos L \\
\quad + \dfrac{v_x}{R_N}\sec^2 L)v_y\delta L + \nabla_x \\
\delta\dot{v}_y = -f_x\sin\phi_z - f_y(\cos\phi_z - 1) \\
\quad -f_z(\phi_y\sin\phi_z - \phi_x\cos\phi_z) \\
\quad -(2\omega_{ie}\sin L + \dfrac{v_x}{R_N}\tan L)\delta v_x \\
\quad -(2\omega_{ie}\cos L + \dfrac{v_x}{R_N}\sec^2 L)v_x\delta L \\
\quad + \nabla_y \\
\dot{\phi}_x = -\dfrac{\delta v_y}{R_M} + (\omega_{ie}\sin L + \dfrac{v_y}{R_M}\tan L)\phi_y \\
\quad -(\omega_{ie}\cos L + \dfrac{v_x}{R_N})\sin\phi_z + \varepsilon_x \\
\dot{\phi}_y = \dfrac{\delta v_x}{R_N} + (1 - \cos\varphi_z)\omega_{ie}\cos L \\
\quad -\omega_{ie}\sin L\delta L - (\omega_{ie}\sin L + \dfrac{v_x}{R_N} \\
\quad \tan L)\phi_x - \dfrac{\delta v_y}{R_M}\sin\phi_z + \varepsilon_y \\
\dot{\phi}_z = \dfrac{\delta v_x}{R_N}\tan L + (\omega_{ie}\cos L + \dfrac{v_x}{R_N} \\
\quad \sec^2 L)\cdot\delta L + (\omega_{ie}\cos L\cos\phi_z \\
\quad + \dfrac{v_x}{R_N})\phi_x - \phi_y\sin\phi_z\omega_{ie}\cos L \\
\quad + \dfrac{v_y}{R_M}\phi_y + \varepsilon_z
\end{cases} \tag{12}$$

Since the vehicle's velocity can also be obtained by the binocular VO system, the velocity difference between the SINS and the VO system is used as the measurement of the SINS/VO integrated navigation system. Thus, the measurement vector is as follows:

$$Z = \begin{bmatrix} v_x^{SINS} - v_x^{VO} \\ v_y^{SINS} - v_y^{VO} \end{bmatrix} \tag{13}$$

Therefore, based on the SINS model and VO model introduced in Section 2, the filter equation can be established as:

$$\begin{cases} X_k = f(X_{k-1}) + G_{k-1}\xi_{k-1} \\ Z_k = H_k X_k + \eta_k \end{cases} \tag{14}$$

wherein the $f(\cdot)$ is the nonlinear state transform matrix while H_k is the measurement matrix; G_{k-1} is the noise driven matrix; ξ_{k-1} and η_k are the process noise and the measurement noise, respectively.

So now we can obtain the $f(\cdot)$ matrix easily from this above differential equation. Meanwhile the measurement matrix can also be derived as follows:

$$H = \begin{bmatrix} 0_{2\times2} & I_{2\times2} & 0_{2\times8} \end{bmatrix} \tag{15}$$

Taken constant and random errors of inertial sensors into account, the process noise vector ξ_{k-1} is:

$$\xi_{k-1} = [0_{1\times2}\ \ w_{ax}\ \ w_{ay}\ \ w_{gy}\ \ w_{gz}\ \ 0_{1\times5}]^\top \tag{16}$$

The noise driven matrix G_{k-1} is where

$$G = \begin{bmatrix} 0_{2\times5} & 0_{2\times2} & 0_{2\times3} & 0_{2\times2} \\ 0_{2\times5} & C_b^{n'}(1) & 0_{2\times3} & 0_{2\times2} \\ 0_{3\times5} & 0_{3\times2} & C_b^{n'} & 0_{3\times2} \\ 0_{5\times5} & 0_{5\times2} & 0_{5\times3} & 0_{5\times2} \end{bmatrix} \tag{17}$$

$$C_b^{n'}(1) = \begin{bmatrix} C_b^{n'}(1,1) & C_b^{n'}(1,2) \\ C_b^{n'}(2,1) & C_b^{n'}(2,2) \end{bmatrix} \tag{18}$$

Based on the above system model, we can use nonlinear filters to estimate the system state, realizing the autonomous navigation for unmanned ground vehicles with the SINS/VO integrated navigation system.

III. AN IMPROVED INTEGRATED NAVIGATION ALGORITHM BASED ON ROBUST H_∞ FILTER AND CKF METHOD

A. THE NONLINEAR CKF METHOD

As we all known, in actual engineering applications, the nonlinear filter should be used. Since the EKF and UKF methods have their limitations, the CKF used the Cubature points based on spherical-radial cubature criterion to approximate the mean and variance of the nonlinear system, getting more and more attention in practical applications.

Considering the nonlinear system:

$$\begin{cases} x_k = f(x_{k-1}) + W_{k-1} \\ z_k = h(x_k) + \eta_k \end{cases} \tag{19}$$

wherein x_k and z_k are the state vector and the measurement vector at time k, respectively; $f(\cdot)$ and $h(\cdot)$ are specific known nonlinear functions; and W_{k-1} and η_k are the noise vectors from two independent zero-mean Gaussian processes with their covariance matrices Q_{k-1} and R_k, respectively.

The set of $2n$ cubature points are given as followed, where ξ_i is the $i-th$ cubature point and ω_i is the corresponding weight.

$$\begin{cases} \xi_i = \sqrt{n}[1]_i \\ \omega_i = \dfrac{1}{2n} \end{cases}, \quad i = 1, 2, \ldots, 2n \tag{20}$$

where n is the dimension of the nonlinear system.

Assume that at time $k-1$ the state estimation $\hat{x}_{k-1|k-1}$ and the matrix of the error covariance $P_{k-1|k-1}$ are already known. The steps involved in the time-update and the measurement-update of the CKF is summarized as follow.

1) Time Update

$$P_{k-1|k-1} = S_{k-1|k-1} S_{k-1|k-1}^{\top} \tag{21}$$
$$X_{i,k-1|k-1} = S_{k-1|k-1} \xi_i + \hat{x}_{k-1|k-1} \tag{22}$$
$$X_{i,k|k-1}^{*} = f\left(X_{i,k-1|k-1}\right) \tag{23}$$
$$\hat{x}_{k|k-1} = \frac{1}{2N} \sum_{i=1}^{2N} X_{i,k|k-1}^{*} \tag{24}$$
$$P_{k|k-1} = \frac{1}{2N} \sum_{i=1}^{2N} X_{i,k|k-1}^{*} X_{i,k|k-1}^{*\top} - \hat{x}_{k|k-1} \hat{x}_{k|k-1}^{\top} + Q_{k-1} \tag{25}$$

2) Measurement Update

$$P_{k|k-1} = S_{k|k-1} S_{k|k-1}^{\top} \tag{26}$$
$$X_{i,k|k-1} = S_{k|k-1} \xi_i + \hat{x}_{k|k-1} \tag{27}$$
$$Y_{i,k|k-1} = h\left(X_{i,k|k-1}\right) \tag{28}$$
$$\hat{y}_{k|k-1} = \frac{1}{2N} \sum_{i=1}^{2N} Y_{i,k|k-1} \tag{29}$$
$$P_{k|k-1}^{zz} = \frac{1}{2N} \sum_{i=1}^{2N} Y_{i,k|k-1} Y_{i,k|k-1}^{\top} - \hat{y}_{k|k-1} \hat{y}_{k|k-1}^{\top} + R_k \tag{30}$$
$$P_{k|k-1}^{xz} = \frac{1}{2N} \sum_{i=1}^{2N} X_{i,k|k-1} Y_{i,k|k-1}^{\top} - \hat{x}_{k|k-1} \hat{y}_{k|k-1}^{\top} \tag{31}$$

Then with the new measurement vector z_k, the blueestimation of the state vector $\hat{x}_{k|k}$ and its covariance matrix $P_{k|k}$ at time k can be obtained by the following equations:

$$K_k = P_{k|k-1}^{xz} \left(P_{k|k-1}^{zz}\right)^{-1} \tag{32}$$
$$\hat{x}_{k|k} = \hat{x}_{k|k-1} + K_k \left(z_k - \hat{z}_{k|k-1}\right) \tag{33}$$
$$P_{k|k} = P_{k|k-1} - K_k P_{k|k-1}^{zz} K_k^{\top} \tag{34}$$

B. NOVEL RHCKF INTEGRATED NAVIGATION ALGORITHM

Although the CKF has a high estimated accuracy, it can be only used when the system noise is already known and Gaussian white noise which is difficult to satisfy in practical systems. So considering the uncertainty of the whole system, the H_∞ filter attracts more and more attentions due to its significant robustness.

In H_∞ filter, the noise is considered as energy-bounded random signal. And after introduced H_∞ norm into estimation framework, this filter is constructed, minimizing the H_∞ norm of the disturbance input and the filter output. Thus, the estimation error has been minimized even worst disturbance exists. So, to solve the nonlinearity and uncertainty of the unmanned ground vehicle system, we proposed a novel robust integrated navigation algorithm, named RHCKF algorithm, based on the robust H_∞ filter and the CKF method in this paper.

Different from minimum variance estimation theory, the robust H_∞ filter guarantees the norm of the transfer function from the input noise to the estimation error to be minimum. It means to minimize the maximum gain from the input signal to the output signal to make the filter has stronger robustness. The cost function is proposed by Huber expressed as:

$$J = \frac{\sum_{k=0}^{N-1} \left(\|e_k\|^{\top} \|e_k\|\right)}{\|X_0 - \hat{X}_0\|_{P_0^{-1}}^2 + \sum_{k=0}^{N-1} \left(\|W_k\|_{Q_k^{-1}}^2 - \|\eta_k\|_{R_k^{-1}}^2\right)} \tag{35}$$

where $\hat{X}_0$ and P_0 denote initial state estimation and estimated error covariance matrix, respectively; e_k is the state estimation error; Positive weighting matrices Q_k and R_k denote the covariance matrix of W_k and η_k, respectively. So the essence of H_∞ filter is expressed as: When P_0, Q_k and R_k reach the upper bound, the estimation strategy is searched to minimize J in order to minimize the estimation error under the circumstance of disturbance maximized.

Generally, the optimal filter solution is difficult to obtain in actual systems, so we can design a suboptimal iterative filtering. We set a robust factor γ of the H_∞ filter which is the upper bound of the pre-determined H_∞ filter performance, yielding:

$$\|J\|_\infty = \sup J \le \gamma^2 \tag{36}$$

According to the Riccati inequation, we get

$$\begin{cases} P_{k|k} = P_{k|k-1} - \left[P_{k|k-1}^{xz} P_{k|k-1}\right] \cdot R_e^{-1} \left[\begin{array}{c} \left(P_{k|k-1}^{xz}\right)^{\top} \\ P_{k|k-1}^{\top} \end{array}\right] \\ R_e = \left[\begin{array}{c} P_{k|k-1}^{zz} \left(P_{k|k-1}^{xz}\right)^{\top} \\ P_{k|k-1}^{xz} P_{k|k-1} - \gamma^2 I \end{array}\right] \end{cases} \tag{37}$$

The generated state distribution from the Cubature points can be controlled utilizing the robust factor γ, so the value of γ has a significant impact on the filtering accuracy and robustness. Smaller γ is, stronger the filtering robustness is. However, for convenience, the γ is generally set based on experiences in practical applications, and is inversely proportional to the innovation.

The procedure of the proposed RHCKF integrated navigation algorithm of the SINS/VO integrated system for unmanned ground vehicles is presented in Table 1. In this improved RHCKF algorithm, the CKF is used to solve the nonlinearity while the H_∞ filter is used to solve the uncertainty in practical systems. Therefore, this RHCKF integrated navigation algorithm not only has the capacity of processing nonlinearity but also is able to achieve great accuracy and robustness.

TABLE 1. Pseudo-code of the RHCKF algorithm.

RHCKF Method	
1	Initialization initial state vector X_0 and initial state variance matrix P_0; initial process noise variance matrix Q_0 and initial measurement noise variance matrix R_0; robust factor γ;
2	$k \geq 1$ a) Time Update Cholesky Decomposition of the variance matrix $P_{k-1\|k-1}$; Calculate the cubature points $X_{i,k-1\|k-1}$; Propagated the cubature points with the nonlinear state equation $X^*_{i,k\|k-1}$ Prediction of the state $\hat{x}_{k\|k-1}$; Prediction of the state error covariance matrix $P_{k\|k-1}$; b) Measurement Update Re-calculate the cubature points $X_{i,k\|k-1}$; Propagated the cubature points with the nonlinear measurment equation $Y_{i,k\|k-1}$; Prediction of the measurement $\hat{y}_{k\|k-1}$; Prediction of the autocorrelation and covariance matrices $P^{zz}_{k\|k-1}$ and $P^{xz}_{k\|k-1}$; c) Estimation of state and covariance matrix Calculate the filter gain and sandwich matrices K_k and R_e; Estimate the state vector; Estimate the covariance matrix;
3	$k = k + 1$, goto and repeat step 2 until the filter ends.

IV. SIMULATION AND EXPERIMENT

A. SIMULATION AND ANALYSIS

The simulation has been done to verify the performance of the proposed RHCKF integrated navigation algorithm. In the simulation, SINS and VO system constitute an integrated navigation system of an unmanned ground vehicle, in which velocity observations are provided by the VO system. And the trajectory of the autonomous unmanned ground vehicle is set as Fig.3 while the true velocity and heading are assumed as Fig.4. The simulation time and sampling interval are 40s and 0.1s, respectively. The performance parameter of the SINS is listed in Table 2.

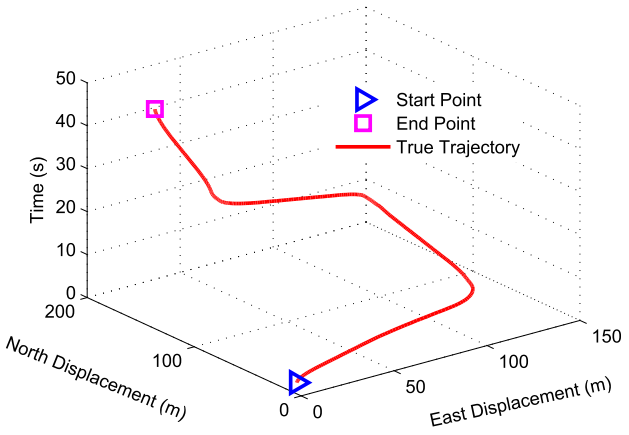

FIGURE 3. True trajectory.

To verify the fault tolerance and robustness of this proposed algorithm, the measurement noise is set as a time-varying

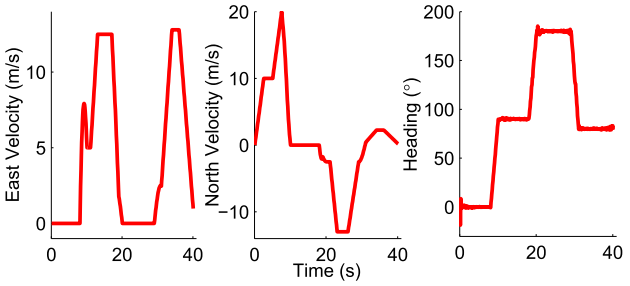

FIGURE 4. True velocity and heading.

TABLE 2. Performance parameters of the SINS.

Parameter		Setting
4*Gyroscope	Constant drift	$0.5°/h$
	Angle random walk	$0.1°/\sqrt{h}$
	Scale factor	100 ppm
	Dynamic range	$\pm 200°/s$
3*Accelerometer	Constant Bias	$10^{-4}g$
	Random noise	$5 * 10^{-5}g$
	Scale factor	100 ppm
	Dynamic range	$\pm 20g$

noise signal. Assume that the variance of the white Gaussian noise η_k is R_0, and the time-varying noise is set as:

$$\eta'_k = \eta_k + 0.5\eta_{k-1} \tag{38}$$

and the corresponding variance of η'_k is

$$\begin{cases} R = R_0, & t \leq 8 \\ R = 1.4R_0, & 8 < t \leq 14 \\ R = 0.8R_0, & 14 < t \leq 40 \end{cases} \tag{39}$$

In this manuscript, to prove the superiority of the novel RHCKF algorithm, traditional CKF method and traditional H_∞ based on EKF method, denote by CKF and HEKF respectively, are taken as references. Monte Carlo simulation has been repeated 20 times and curves of the positioning error, velocity error and the heading error are expressed as Fig.5, Fig.6 and Fig.7, respectively. In these figures, the black dash

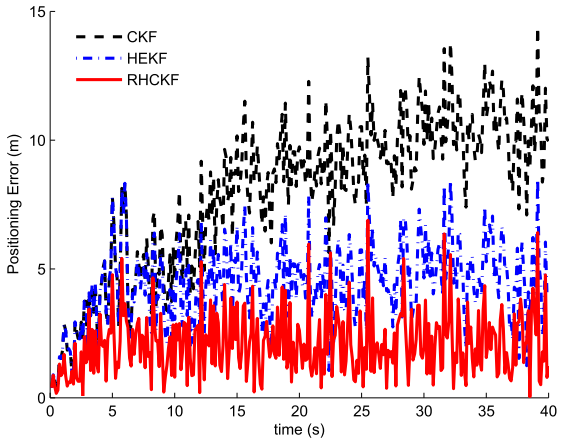

FIGURE 5. Curves of positioning errors.

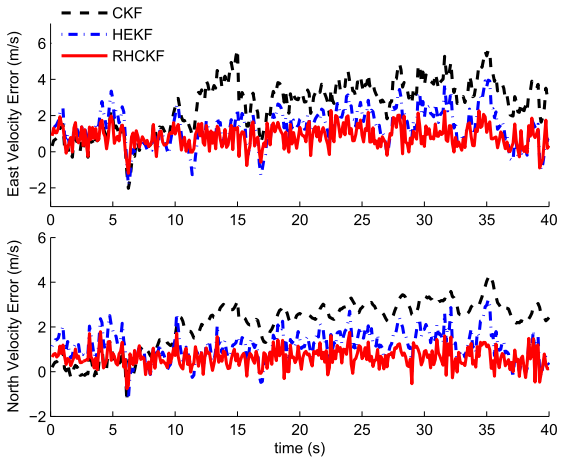

FIGURE 6. Curves of velocity errors.

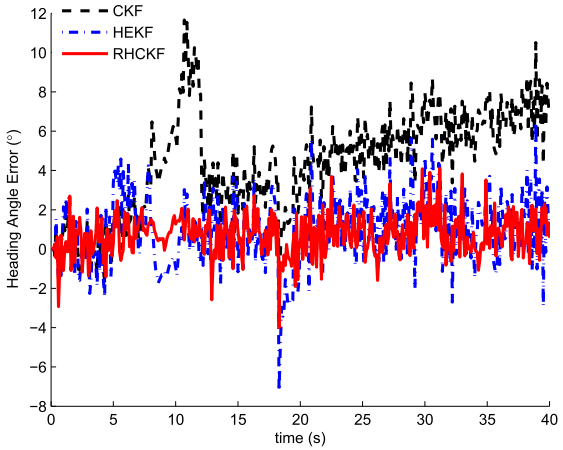

FIGURE 7. Curves of heading angle errors.

line, the blue dash-dot line and the red solid line describe errors of the CKF algorithm, the HEKF algorithm and the RHCKF algorithm, respectively.

From Fig.5 to Fig.7, we can see that the position error, the velocity errors and the haeding errors are also suddenly become larger after 4s and the error curves are fluctuant after 4s with the traditional CKF method. Correspondingly, with the HEKF and RHCKF methods, the fluctuation are smaller. So we can know that the HEKF and RHCKF methods can deal with the system uncertainty availably. And the largest position errors with HEKF and RHCKF methods are about 8.5m and 5.9m, respectively; the east largest velocity errors with HEKF and RHCKF methods are 3.9m/s and 2.1m/s while the north velocity errors are 2.7m/s and 1.9m/s; the heading errors with HEKF and RHCKF methods are $-7.1°$ and $4.1°$, respectively. So we can know that clearly the RHCKF algorithm has better robustness.

In order to quantitative analyze the performance of these three algorithms, the mean and the standard deviation of errors are calculated and summarized in Fig.8.

From Fig.8, it is obviously that means and standard deviations of the heading error, east velocity error, north velocity and positioning error with the traditional CKF algorithm are the largest. Between HEKF and RHCKF algorithms, corresponding errors with the proposed novel RHCKF algorithm are smaller. Means of heading angle, velocity and position with RHCKF algorithm are reduced almost 20%, 50%, 50%, and 50%. So we can see that the proposed RHCKF integrated navigation algorithm has a better performance than the CKF and REKF algorithms on the filtering accuracy and robustness.

To evalutate the efficiency of these three algorithms further, their computational times are compared. The simulation was processed by MATLAB 2018a on the same computer equipped with an AMD A10-9600P RADEON R5, 10 COMPUTE CORES 4C+6G, 2.40GHz processor and 4GB RAM under Windows 10. To make the comparison more intuitive, assumed that the computational time of the trodtioanl CKF algorithm is 1, relatively computational times of HEKF and RHCKF algorithm are 1.212 and 1.317, respectively. So the traditional CKF algorithm is the simplest and fastest algorithm among these three algorithm, the HEKF algorithm takes the second place, and the RHCKF algorithm is slower approximate 31.7% than CKF algorithm due to its calculation of the weighted matrix. So from above analysis, we can see that the RHCKF can obtain high accuracy and better robustness at the cost of a certain degree of computational times, which can be acceptted.

B. REAL DATA TEST AND ANALYSIS

In order to verify the effectiveness of the novel RHCKF method based on the H_∞ filter and the CKF, a real data from the Karlsruhe Institute of Technology and Toyota Technological Institute (KITTI) Vision Benchmark Suite is used here [30], [31]. The KITTI data set is the largest evaluation data set of the computer vision algorithm in the world under automatic driving scenarios, including the urban, rural and highway scenes, with varying degrees of shadings. In this open database, the recording platform is Volkswagent Passat B6, which has been modified with actuators. The outlook of the unmanned vehicle is shown as Fig.9 and various sensors are installed on it. One inertial and GPS navigation system (GPS/IMU) OXTS RT 3003, a Laserscanner Velodyne HDL-64E, 2 PointGray Flea2 grayscale cameras (FL2-14S3M-C) and 4 Varifocal lenses are equipped. Accurate ground truth is provided by the Velodyne laser scanner and the GPS localization system. Performance parameters of the OXTS RT 3003 are listed in Table 3 and Table 4. Two FL2-14S3M-C grayscale cameras constitute a VO system and offers the observation and the performance of the VO system is analyzed in [7]. The data is recorded using an eight core i7 computer, and the sampling frequency is 10Hz.

Considering that trees and the illumination variant in the residential area will interfere with the camera observation, making the actual system uncertainty, a set of residential area data, named Dataset 0033, is used here. In this data set, there are 1594 pair of images, which are all calibrated and synchronized. The size of each image is approximately

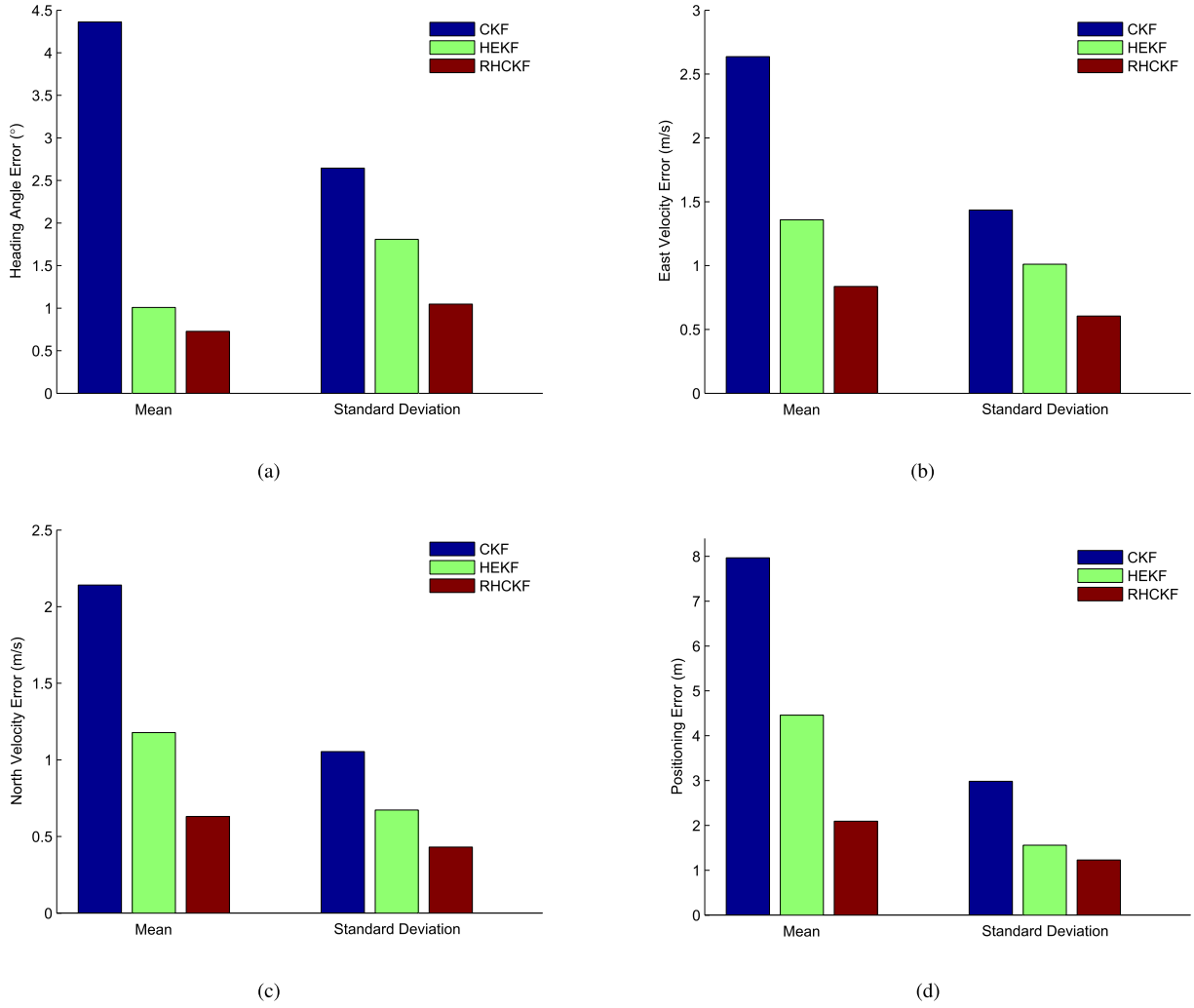

FIGURE 8. Means and standard deviations with different algorithms. (a) Comparison of heading angle estimation. (b) Comparison of east velocity estimation. (c) Comparison of north velocity estimation. (d) Comparison of positioning estimation.

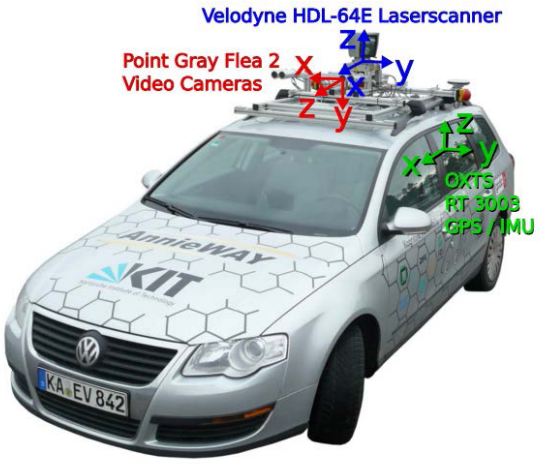

FIGURE 9. Outlook of the unmanned vehicle.

1242 × 375 pixels. The true trajectory of this experimental data is shown as Fig.10. Since that the means and standard deviations of the east velocitu error, the north velocity error

TABLE 3. Technical specifications of OXTS RT 3003.

Parameter	Performance
Position accuracy (CEP)	1.5m/SPS; 0.01m/RTK
Velocity accuracy (RMS)	0.05 km/h
Pitch/Roll accuracy (1σ)	0.03 °
Heading accuracy (1σ)	0.1°
Track angle accuracy (1σ)	0.07°
Slip angle accuracy (1σ)	0.15°
Frequency	$10Hz$

and the positioning eror of this data set are already analyzed in details in [7], we use the velocity obtained by the VO system as the measurement directly.

The proposed RHCKF algorithm is used to estimate the system state while the normal CKF and HEKF algorithms are also as references. And positioning errors of the autonomous driving car with different algorithms are shown in Fig.11 while their means and standard deviations are shown in Fig.12.

From Fig.11, we can see that: the positioning error with CKF algorithm increases quickly and the maximum

TABLE 4. Performance parameters of OXTS sensors.

Parameter		Performance
5*Gyroscope	Bias stability	$2^\circ/h$
	Linearity	0.05%
	Scale factor	0.1%
	Dynamic range	$\pm 300^\circ/s$
	Random walk	$0.2^\circ/\sqrt{h}$
5*Accelerometer	Bias stability	$2\mu g$
	Linearity	0.01%
	Scale factor	0.1%
	Dynamic range	$\pm 30g$
	Random walk	$0.005m/s/\sqrt{h}$

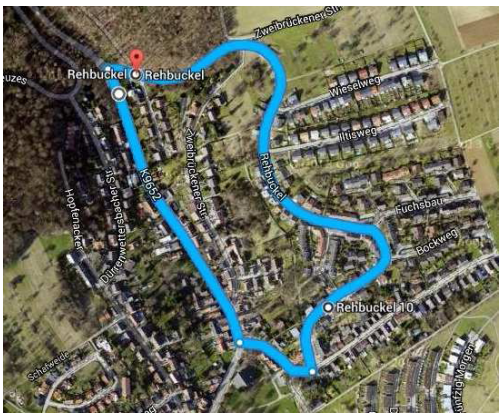

FIGURE 10. True trajectory.

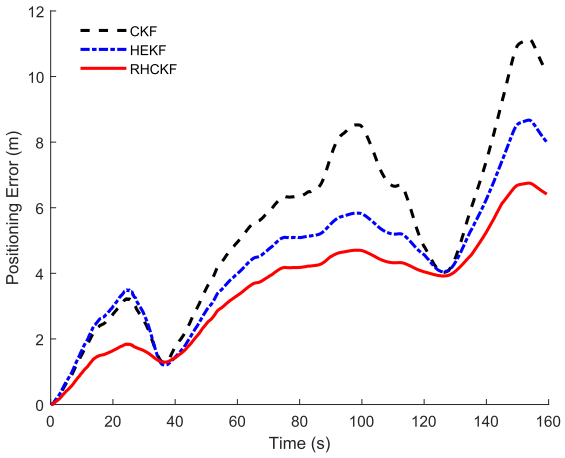

FIGURE 11. Comparison of positioning errors.

is about 11.14m, with the RHCKF integrated navigation algorithm the positioning error is smallest and its maximum is only about 6.75m; and the positioning error with the HEKF algorithm is about 8.67m. Thus, the maximum of positioning error with the RHCKF integrated navigation algorithm is reduced nearly 39.4%. Then Fig.12 gives the mean and the standard deviation with these three algorithm, and the RHCKF algorithm has the smallest value. Therefore, the superiority of the proposed the RHCKF integrated navigation algorithm is verified.

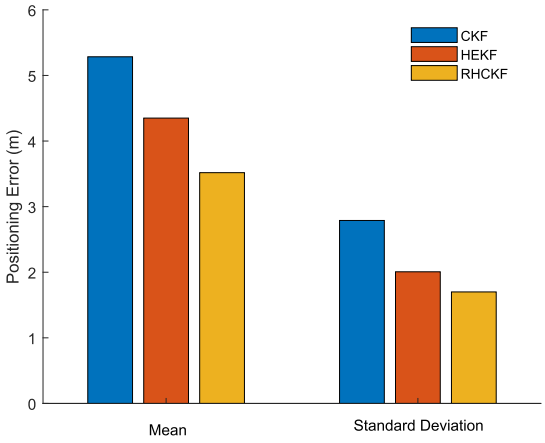

FIGURE 12. Means and standard deviations of positioning errors.

V. CONCLUSIONS

In order to enhance the localization accuracy of unmanned ground vehicles in the GNSS denied environment, a novel robust localization algorithm based on the robust H_∞ filter and nonlinear CKF method is proposed, named RHCKF algorithm, in this manuscript. On the basis of the established mathematical models of the SINS and the binocular camera VO system, the framework of the SINS/VO integrated navigation system was set up firstly. Secondly, a robust nonlinear filter based on the robust H_∞ filter and nonlinear CKF was proposed. Finally, simulations and real test are both utilized to verify the performance of this novel novel integrated navigation algorithm. Results showed that with this proposed RHCKF algorithm the positioning accuracy and robustness of the SINS/VO integrated navigation system can be enhanced availably at the cost of a litter computation time which can be acceptted.

REFERENCES

[1] C. Melendez-Pastor, R. Ruiz-Gonzalez, and J. Gomez-Gil, "A data fusion system of GNSS data and on-vehicle sensors data for improving car positioning precision in urban environments," *Expert Syst. Appl.*, vol. 80, pp. 28–38, Sep. 2017.

[2] Y.-J. Liu, C.-C. Chiu, and J.-H. Yang, "A robust vision-based skyline detection algorithm under different weather conditions," *IEEE Access*, vol. 5, pp. 22992–23009, 2017.

[3] A. Volkova and P. W. Gibbens, "More robust features for adaptive visual navigation of UAVs in mixed environments," *J. Intell. Robotic Syst.*, vol. 90, nos. 1–2, pp. 171–187, 2018.

[4] T. T. Mac, C. Copot, R. De Keyser, and C. M. Ionescu, "The development of an autonomous navigation system with optimal control of an UAV in partly unknown indoor environment," *Mechatronics*, vol. 49, pp. 187–196, Feb. 2018.

[5] Q. Sun, Y. Zhang, J. Wang, and W. Gao, "An improved FAST feature extraction based on RANSAC method of vision/SINS integrated navigation system in GNSS-denied environments," *Adv. Space Res.*, vol. 60, no. 12, pp. 2660–2671, 2017.

[6] G. Sun, M. Wang, and L. Wu, "Unexpected results of extended fractional Kalman filter for parameter identification in fractional order chaotic systems," *Int. J. Innov. Comput., Inf. Control*, vol. 7, no. 9, pp. 5341–5352, 2011.

[7] Q. Sun, M. Diao, Y. Li, and Y. Zhang, "An improved binocular visual odometry algorithm based on the random sample consensus in visual navigation systems," *Ind. Robot*, vol. 44, no. 4, pp. 542–551, 2017.

[8] G. Sun and Z. H. Zhu, "Fractional-order tension control law for deployment of space tether system," *J. Guid., Control, Dyn.*, vol. 37, no. 6, pp. 2057–2062, 2014.
[9] D. Caruso, A. Eudes, M. Sanfourche, D. Vissière, and G. L. Besnerais, "A robust indoor/outdoor navigation filter fusing data from vision and magneto-inertial measurement unit," *Sensors*, vol. 17, no. 12, p. 2795, 2017.
[10] J.-C. Piao and S.-D. Kim, "Adaptive monocular visual–inertial SLAM for real-time augmented reality applications in mobile devices," *Sensors*, vol. 17, no. 11, p. 2567, 2017.
[11] Y. Wang, X. Hu, L. Zhang, J. Lian, and X. He, "Polarized light compass-aided visual-inertial navigation under foliage environment," *IEEE Sensors J.*, vol. 17, no. 17, pp. 5646–5653, Sep. 2017.
[12] P. B. S. Harsha and D. V. Ratnam, "Implementation of advanced carrier tracking algorithm using adaptive-extended Kalman filter for GNSS receivers," *IEEE Geosci. Remote Sens. Lett.*, vol. 13, no. 9, pp. 1280–1284, Sep. 2016.
[13] Z. Gao, D. Mu, S. Gao, Y. Zhong, and C. Gu, "Adaptive unscented Kalman filter based on maximum posterior and random weighting," *Aerosp. Sci. Technol.*, vol. 71, pp. 12–24, Dec. 2017.
[14] W. Gao, Y. Zhang, and J. Wang, "A strapdown interial navigation system/beidou/Doppler velocity log integrated navigation algorithm based on a cubature Kalman filter," *Sensors*, vol. 14, no. 1, pp. 1511–1527, 2014.
[15] B. Cui, X. Chen, X. Yuan, H. Huang, and L. Xiao, "Performance analysis of improved iterated cubature Kalman filter and its application to GNSS/INS," *ISA Trans.*, vol. 66, pp. 460–468, Jan. 2016.
[16] Q. Li and F. Sun, "Strong tracking cubature Kalman filter algorithm for GPS/INS integrated navigation system," in *Proc. IEEE Int. Conf. Mechatron. Automat.*, Aug. 2013, pp. 1113–1117.
[17] L. Zhang, S. Li, E. Zhang, and Q. Chen, "Robust measure of non-linearity-based cubature Kalman filter," *IET Sci., Meas. Technol.*, vol. 11, no. 7, pp. 929–938, Oct. 2017.
[18] C. Niu, Y. Li, R. Q. Hu, and F. Ye, "Fast and efficient radio resource allocation in dynamic ultra-dense heterogeneous networks," *IEEE Access*, vol. 5, pp. 1911–1924, 2017.
[19] Q. Sun, Y. Tian, and M. Diao, "Cooperative localization algorithm based on hybrid topology architecture for multiple mobile robot system," *IEEE Internet Things J.*, to be published.
[20] J. Liu, B.-G. Cai, and J. Wang, "Cooperative localization of connected vehicles: Integrating GNSS with DSRC using a robust cubature Kalman filter," *IEEE Trans. Intell. Transp. Syst.*, vol. 18, no. 8, pp. 2111–2125, Aug. 2017.
[21] M. Zhong, J. Guo, D. Guo, and Z. Yang, "An extended H_i/H_∞ optimization approach to fault detection of INS/GPS-integrated system," *IEEE Trans. Instrum. Meas.*, vol. 65, no. 11, pp. 2495–2504, Nov. 2016.
[22] D. A. Medina, M. Romanovas, I. Herrera-Pinzón, and R. Ziebold, "Robust position and velocity estimation methods in integrated navigation systems for inland water applications," in *Proc. Position, Location Navigat. Symp.*, Apr. 2016, pp. 491–501.
[23] X. Zhao, P. Shi, and X. Zheng, "Fuzzy adaptive control design and discretization for a class of nonlinear uncertain systems," *IEEE Trans. Cybern.*, vol. 46, no. 6, pp. 1476–1483, Jun. 2016.
[24] X. Zhao, X. Wang, G. Zong, and H. Li, "Fuzzy-approximation-based adaptive output-feedback control for uncertain non-smooth nonlinear systems," *IEEE Trans. Fuzzy Syst.*, to be published.
[25] H. Wang, H. R. Karimi, P. X. Liu, and H. Yang, "Adaptive neural control of nonlinear systems with unknown control directions and input dead-zone," *IEEE Trans. Syst., Man, Cybern. Syst.*, to be published.
[26] H. Wang, P. X. Liu, S. Li, and D. Wang, "Adaptive neural output-feedback control for a class of nonlower triangular nonlinear systems with unmodeled dynamics," *IEEE Trans. Neural Netw. Learn. Syst.*, vol. 29, no. 8, pp. 3658–3668, Aug. 2018.
[27] K. Zhu, J. Zhao, and Y. Liu, "H_∞ filtering for switched linear parameter-varying systems and its application to aero-engines," *IET Control Theory Appl.*, vol. 10, no. 18, pp. 2552–2558, Dec. 2016.
[28] F. Liu, Y. Balazadegan, and Y. Gao, "Tight integration of INS/stereo VO/digital map for land vehicle navigation," *Photogramm. Eng. Remote Sens.*, vol. 84, no. 1, pp. 15–23, 2018.
[29] W. Li *et al.*, "Real-time location-based rendering of urban underground pipelines," *Int. J. Geo-Inf.*, vol. 7, no. 1, p. 32, 2018.
[30] A. Geiger, P. Lenz, C. Stiller, and R. Urtasun, "Vision meets robotics: The KITTI dataset," *Int. J. Robot. Res.*, vol. 32, no. 11, pp. 1231–1237, 2013.
[31] M. Menze and A. Geiger, "Object scene flow for autonomous vehicles," in *Proc. Conf. Comput. Vis. Pattern Recognit. (CVPR)*, Jun. 2015, pp. 3061–3070.

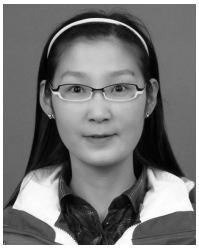

YA ZHANG received the B.Eng. and Ph.D. degrees from Harbin Engineering University, Harbin, Heilongjiang, China, in 2010 and 2015, respectively. She currently holds a post-doctoral position at the School of Electrical Engineering and Automation, Harbin Institute of Technology, Harbin. Her current research interests include vision-based mobile robot navigation systems and multi-sensor information fusion.

FEI YU received the B.S. degree from the Dalian University of Technology in 1997 and the M.Eng. and Ph.D. degrees from Harbin Engineering University, Harbin, China, in 2003 and 2005, respectively. He is currently a Professor with the School of Electrical Engineering and Automation, Harbin Institute of Technology. His current research interests include inertial navigation systems.

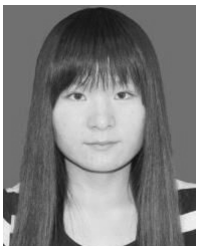

YANYAN WANG received the B.Eng. degree from Harbin Engineering University, Harbin, China, in 2015. She is currently pursuing the Ph.D. degree with the School of Electrical Engineering and Automation, Harbin Institute of Technology. Her current research interests include inertial navigation and integrated navigation systems.

KAI WANG received the B.Eng. degree from the Harbin Institute of Technology in 2017, where he is currently pursuing the M.Eng. degree with the School of Electrical Engineering and Automation. His current research interests include inertial navigation and inertial measurement.